JOURNAL OF APPLIED CRYSTALLOGRAPHY

Volume 51 (2018)

Supporting information for article:

μCHILL – A lightweight, modular system for handling crystalline samples at low temperatures under inert conditions

Michael Solar and Nils Trapp

Supporting information

S1. List of build materials (assemblies C/D)

- 3D printed parts (PLA or PETG)
- Standard issue microscopy slides (75.5x25.4x1.0mm, beveled corners recommended)
- 40x40x2 aluminum U profile
- 25 mm OD PVC pipe (cold gas)
- 8 mm OD PVC pipe (shroud gas feed, optional stabilizers)
- 6 mm OD PU hose (thermocouple guide, shroud gas feed)
- PU construction foam
- Needle valve with fittings (temp control)
- Matching Y splitter (6 mm to 2x8 mm shown in Figures)
- Thermocouple with wire (2 mm diameter recommended for good fit)
- Thermocouple readout
- M4 hex nuts
- M4x6 socket head button screws
- M4 washer (1x, for pin holder locking lever)
- M4x8 hex head cap screw (1x, for pin holder locking lever)
- Cylindrical magnet (e.g. 3.5x7mm, for pin holder)

Tools: painters tape, Allen keys, hacksaw, cutter or hobby knife, small pliers

Overall estimated cost for variants C/D (including all parts as shown except Dewar vessel): < 30 USD
Total estimated assembly time: < 1 hour + foam setting time

Assembly instructions: muCHILL_assembly.pdf
Annotated list of available 3D-printable parts: muCHILL_partslist.pdf
3D print files in .stl format: muCHILL_printfiles.zip

S2. Additional images and plots

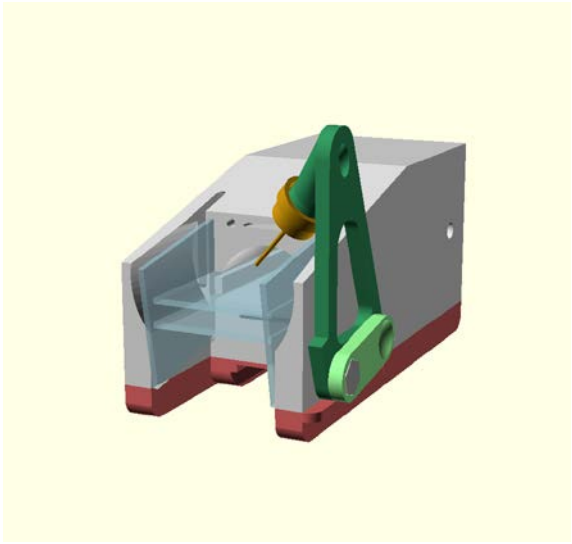

Figure S1 µCHILL coldhead with mounted accessories: Rotating magnetic pin holder (dark green, locked in upright position, locking lever in light green and magnetic pin shown in bronze color), parametric spacer with dovetail slide for further attachments (red, height can be adjusted before print). Attachments are also available in left-handed configuration.

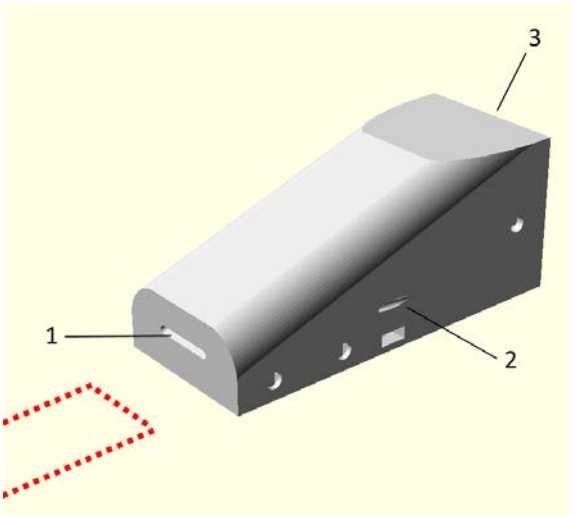

Figure S2 Alternate coldhead using the working principle of X-Temp 2 (Kottke & Stalke, 1993), using a pressurized air loop around the nozzle instead of a resistance heater. 1 – cold gas nozzle (thermal probe port positioned inside the head near to the outlet, must be calibrated against the actual temperature on the work zone), 2 – pressurized air outlet from heater loop, 3 – connections and fittings are identical to the µCHILL coldhead (Figure 1) and compatible with all other modular components. The work zone is highlighted in red.

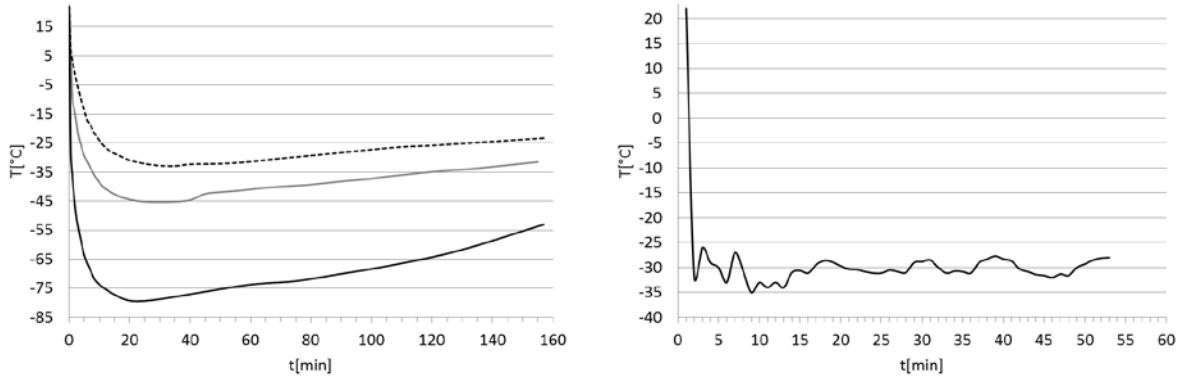

Figure S3 Temperature profiles for variant C, exactly as shown in Figure 2, with a splitter and valve between shroud and cold gas inlet (pressure fixed at 1 bar). Temperatures were measured with a K-type thermocouple directly in the work zone center on the glass surface (when using an inbuilt probe, calibration curves must be recorded unless the probe touches the glass surface). Left: Exemplary temperature decay at three different initial temperatures. The control valve was adjusted only initially and then left untouched during the process, to demonstrate the long-term stability. Runtime exceeded 160 minutes in all cases without refilling LN_2. Right: Exemplary working with quick cooldown to the target temperature (–30°C, control valve initially fully open). Only small adjustments were made subsequently (every 5-15 minutes) whenever the temperature increased by more than 2°C.

S3. Case study: Structure redetermination of $LiBH_4$

X-ray single crystal structures were measured on a Rigaku Oxford Diffraction XtaLAB Synergy-S dual source kappa diffractometer equipped with a Dectris Pilatus 300 HPAD detector and using microfocus sealed tube Cu-Kα radiation with mirror optics (λ = 1.54178 Å). Both measurements were carried out at 100K using an Oxford Cryosystems Cryostream 800 sample cryostat. The detector is free of electronic noise, and in combination with the very intense Cu radiation delivered by the microbeam source any occurring ice formation would immediately be detected as increased background, powder rings or discrete reflections. None of these phenomena were observed in either measurement (short exposure times were chosen to avoid masking by increased background).

Data were integrated using CrysAlisPro and corrected for absorption effects using empirical corrections (ABSPACK, Rigaku, 2016). The structures were solved using Superflip (Palatinus *et al.*, 2007 & 2012) and refined by full-matrix least-squares analysis (SHELXL, Sheldrick, 2008 & 2015) using the program package OLEX2 (Dolomanov *et al.*, 2009). Li and B atoms were refined anisotropically, hydrogen atoms were refined with isotropic parameters. No distance restraints or

constraints were applied. The included .cif files include full metadata, model parameters, crystal face descriptions and structure factors.

The following section describes a typical exemplary working procedure:

A few mg of $LiBH_4$ as supplied by the manufacturer and permanently stored in an argon glovebox were transferred to a Schlenk tube. The vessel was removed from the glovebox, connected to a nitrogen feed and placed with its opening close to the μCHILL coldhead, which was preset and stabilized at –30°C. A thermally insulated needle tip was dipped in low-viscosity perfluoropolyalkylether (ABCR, 7 cSt.) and precooled on the coldhead. The Schlenk vessel was opened, maintaining a steady nitrogen flow to protect the contents. Subsequently some $LiBH_4$ was picked up in the cold oil on the needle tip, then transferred from the vessel to the work zone on the glass slide. The first crystal was chosen and prepared for immediate measurement (beginning approximately 5 min after switching on the cold gas flow). After one hour, during which the temperature had increased to –28°C, the second crystal (chosen for similar size) was prepared and measured in the same manner (Figure S4). In both cases, after cleaning and placing the crystals on a Kapton sample holder (MiTeGen), the sample was quickly carried to the diffractometer relying on the perfluoropolyalkylether oil film for short-term protection (< 10 sec transfer time, diffractometer cryostat pre-cooled to 100 K). No ice formation was observed on raw frames or reconstructed precession images (Figure S5).

Even though the crystals visually appeared to be of poor quality, publication-grade data were obtained in both cases with very similar quality indicators (Table S1 and enclosed .cif files). Raw images and reciprocal space reconstructions showed no signs of ice formation (Figure S5). After two hours, crystals remaining on the μCHILL device still appeared undamaged. As a final control experiment, the device was first warmed up to room temperature by closing the evaporator control valve and then switched off entirely. Decomposition could be detected visually already after 10 min, even though the sample was still covered in a thick layer of protective oil. Violent bubble formation and total decomposition occurred approximately after 30 min (Figure S6).

Table S1 Data collection statistics for $LiBH_4$ crystals #1 and #2 in comparison with a reported synchrotron data set. The authors also used crystals as supplied by the manufacturer. Hydrogen atoms were refined anisotropically in the original work.

	Crystal #1	Crystal #2	Filinchuk *et al.*, 2008
Temperature [K]	100.0(1)	100.0(1)	225(1)
Crystal system	orthorhombic	orthorhombic	orthorhombic
Space group	*Pnma*	*Pnma*	*Pnma*
a [Å]	7.1374(7)	7.1431(6)	7.141(5)
b [Å]	4.4172(5)	4.4159(4)	4.431(3)
c [Å]	6.7029(8)	6.7027(6)	6.748(4)
V [Å^3]	211.33(4)	211.42(3)	213.5(2)
Z, ρ_{calc} [g/cm^3]	4, 0.685	4, 0.684	4, 0.678
Crystal size [mm^3]	0.13×0.08×0.06	0.14×0.09×0.06	~0.2 mm
Radiation	CuKα (λ=1.54184)	CuKα (λ=1.54184)	Synchrotron (λ=0.71118)
μ [mm^{-1}]	0.094	0.094	0.021
$2\theta_{max}$ [°]	132.0	132.0	48.8
Completeness [%]	99.1	99.5	99.0
R_{int}, R_σ	0.0307, 0.0422	0.0366, 0.0388	0.045, 0.027
reflns collected, unique	527, 209	482, 210	2161, 200
data/restraints/parameters	209/0/23	210/0/23	200/0/34
final R indices, [$I > 2\sigma(I)$]	R_1 = 0.0560 wR_2 = 0.1358	R_1 = 0.0521 wR_2 = 0.1274	R_1 = 0.0455 wR_2 = 0.1318
R indices (all data)	R_1 = 0.0581 wR_2 = 0.1381	R_1 = 0.0552 wR_2 = 0.1292	R_1 = 0.0459 wR_2 = 0.1326
Goodness-of-fit on F^2	1.155	1.133	1.175
largest Fourier diff (eÅ^{-3})	0.16, -0.10	0.22, -0.12	0.11, -0.12
B-H [Å]	1.1102(1)-1.1235(1)	1.1101(1)-1.1354(1)	1.104(11)-1.131(15)

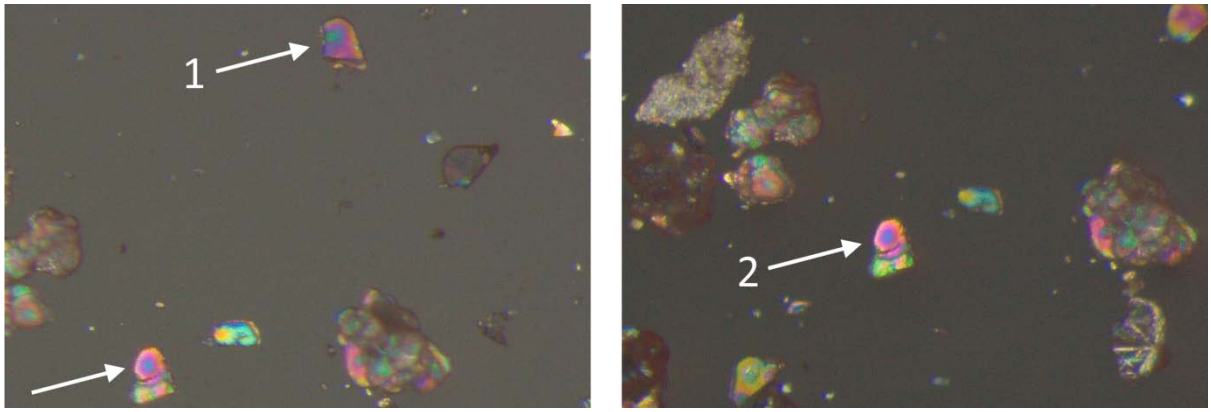

Figure S4 Polarized light microscopic images (50× magnification) of low quality $LiBH_4$ crystals in μCHILL work zone. Images are entirely unobstructed by the cold gas stream. The sample was picked with a drop of pre-cooled low-viscosity perfluoropolyalkylether oil (ABCR, 7 cSt.) from a Schlenk vessel connected to a dry N_2 feed. Left: Initial image at –30°C directly after sample transfer. Crystals for both measurements are highlighted. Crystal #1 was subsequently transferred to a Kapton mount, removed from the μCHILL and quickly carried to the diffractometer for measurement. Right: Image at –28°C, taken after one hour and without further intervention (some drifting was observed). Note that crystal #2 remains visually undamaged and no bubble formation occurred in the surrounding material. The crystal was cleaned of debris and transferred to the diffractometer in the same manner as crystal #1. Crystal dimensions for reference, in mm: #1: 0.06×0.08×0.13, #2: 0.06×0.09×0.14.

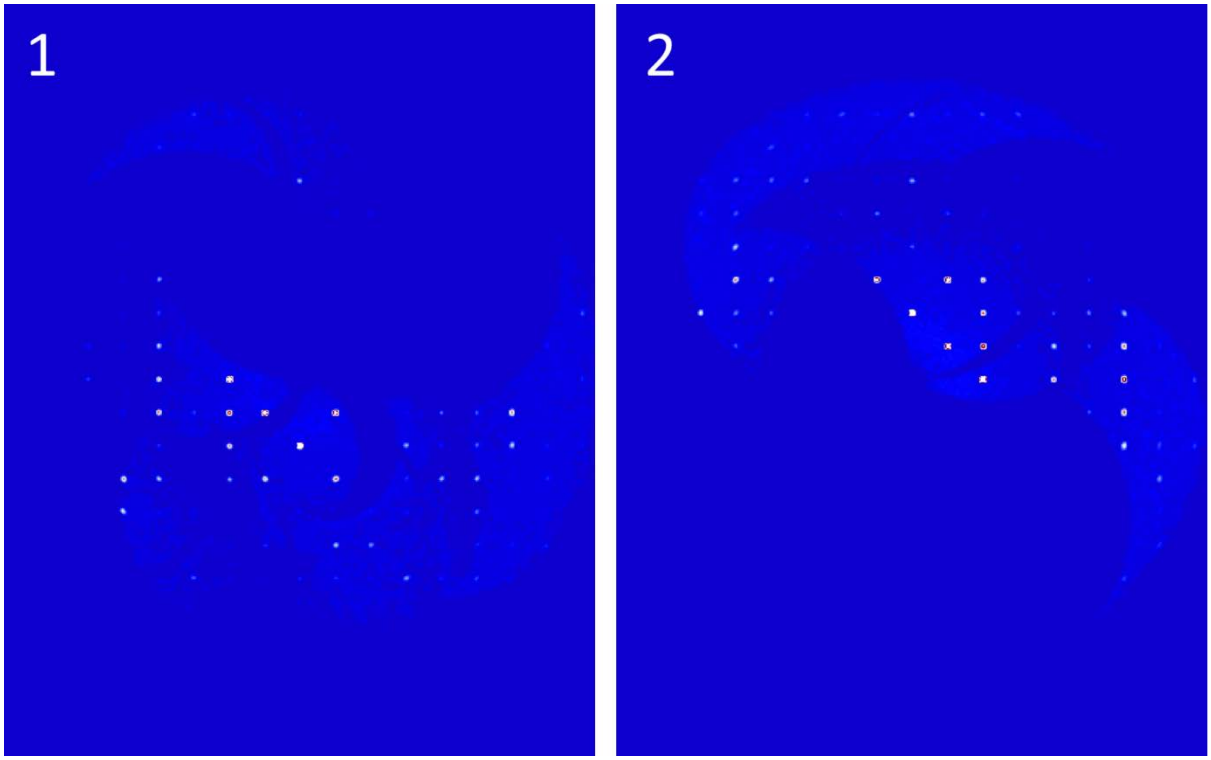

Figure S5 Reconstructed precession images from X-ray structure measurements of crystals #1 and #2 (Cu radiation, 100K, 0KL plane, primary beam impact at image centers). The highest possible contrast settings were applied. No rings or increased background indicative of ice formation are observed.

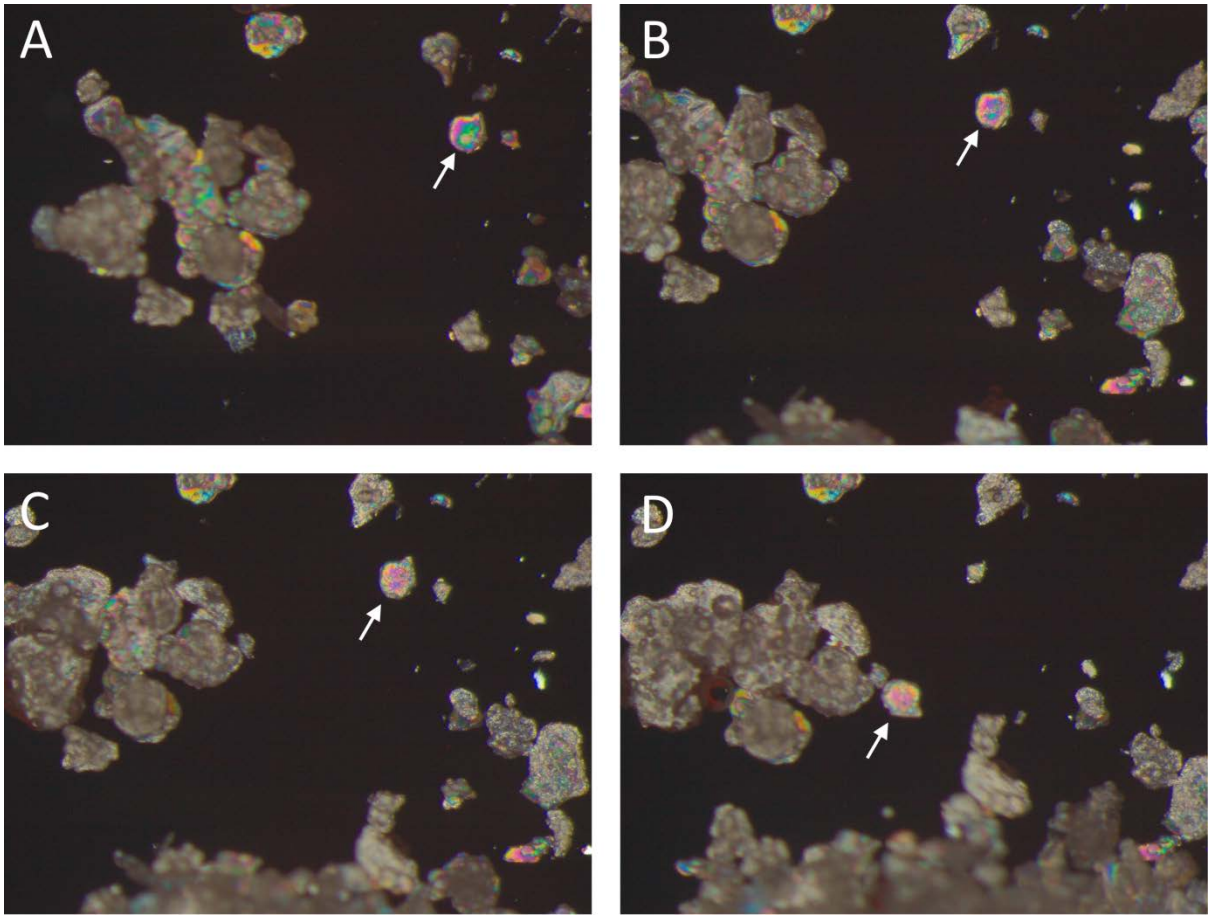

Figure S6 Polarized light microscopic images (50× magnification) of $LiBH_4$ crystals and amorphous material (random section) in final control experiment (decomposition test). A: Before switching off the cold gas and shroud flow (following 2 h of uninterrupted operation at –30°C and subsequent warming to RT). B: After 10 min, even though protected by a thick layer of perfluoropolyalkylether oil, the sample already shows bubble formation. The indicated crystal becomes noticeably turbid. C: After 20 min, rapid bubble formation is observed in the amorphous material bulk. The indicated crystal has become opaque and its surface is damaged by microbubble formation. D: After 30 min, violent bubble formation is observed and material starts drifting rapidly. Immediately after taking this picture the indicated crystal and most other material deformed entirely.

References

Kottke, T. & Stalke, D. (1993). *J. Appl. Cryst.* **26**, 615–619.

CrysAlisPro and ABSPACK (2016). Rigaku Oxford Diffraction.

Palatinus, L. & Chapuis, G. (2007). *J. Appl. Cryst.* **40**, 786–790.

Palatinus, L., Prathapa, S. J. & van Smaalen, S. (2012). *J. Appl. Cryst.* **45**, 575–780.

Sheldrick, G. M. (2008). *Acta Cryst.* **A64**, 112–122.

Sheldrick, G. M. (2015). *Acta Cryst.* **C71**, 3–8.

Dolomanov, O. V., Bourhis, L. J., Gildea, R. J., Howard, J. A. K., Puschmann, H. (2009). *J. Appl. Cryst.* **42**, 339–341.

Filinchuk, Y., Chernyshov, D. & Cerny, R. (2008). *J. Phys. Chem. C* **112**, 10579–10584.